energies

MDPI

Article

Numerical Study on the Mechanism of Coal and Gas Outburst in the Coal Seam Thickening Area during Mining

Zhengshuai Liu [1,2], Longyong Shu [2,*], Zhonggang Huo [2] and Yongpeng Fan [2]

[1] Chinese Institute of Coal Science, Beijing 100013, China; lzsfxy@163.com
[2] China Coal Research Institute, Beijing 100013, China
* Correspondence: slyccri@163.com

Abstract: Most coal and gas outbursts occur in the coal thickness variation zone. However, it is difficult to illustrate the mechanism of outbursts in coal thickening areas by physical simulation experiments. In this study, a coupled multi-field model, established by considering the stress–strain field, gas transport field and damage field, was used to investigate the evolution of stress, gas pressure and plastic failure zones under different variation gradients and amplitudes of coal thickness. The simulation results show that the stress peak at the coal thickening transition zone caused by mining is higher than that at the constant thickness coal seam. The stress peak at the coal thickening transition zone decreases from 18.8 MPa to 16.9 MPa with the increase in the transition zone from 0 m to 10 m under the constant coal thickness variation from 3 m to 7 m; while it increases from 16.2 MPa to 19.3 MPa with the increase in the transition zone from 2 m to 10 m under the constant coal thickness variation gradient of 45°. Similarly, the plastic deformation volume of the coal seam between the driving face and the coal thickening interface increases with the increase in the coal thickness variation gradient and amplitude. In addition, the gas pressure in the fracture declines slower in the coal thickness variation zone affected by the higher coal thickness variation gradients or amplitudes. The mechanism for outbursts occurring in the increasing coal thickness area was further discussed, and combined with the simulation results for the energy principle of outbursts. Compared with the constant thickness coal seam, the elastic energy increases from 1.85 MJ to 1.94 MJ, and the free gas expansion energy increases from 24.19 MJ to 50.57 MJ when the coal thickness varies from 3 m to 13 m within a 10 m transition zone. The variation of coal thickness causes higher stress, higher gas pressure and low coal strength, which triggers outbursts more easily. The research could provide the theoretical support to prevent and control outbursts in coal seam thickening areas during mining.

Keywords: coal and gas outburst; coal thickness variation; mining stress; gas pressure; outburst energy

Citation: Liu, Z.; Shu, L.; Huo, Z.; Fan, Y. Numerical Study on the Mechanism of Coal and Gas Outburst in the Coal Seam Thickening Area during Mining. *Energies* **2023**, *16*, 3288. https://doi.org/10.3390/en16073288

Academic Editor: Krzysztof Skrzypkowski

Received: 10 March 2023
Revised: 29 March 2023
Accepted: 4 April 2023
Published: 6 April 2023

1. Introduction

Coal as a non-renewable energy source is still a dominant type of energy consumption in China, and its exploitation plays an essential role in energy support. However, coal and gas outbursts (hereafter as "outbursts") are among the most dangerous disasters that can occur during mining, which not only influences coal exploitation, but also threatens the safety of personnel [1]. Moreover, the probability of outburst accidents increases with the increase in mining depth [2]. Thus, the mechanism, prevention and control of outbursts has been a focus for research worldwide. Previous research has shown that the occurrence of outbursts is due to the comprehensive role of the stress factor, gas factor and coal body factor [3–5]. Based on field locations where outbursts had occurred, Shu et al. [6] proposed a novel idea that the outbursts mainly occurred in a special geological structural environment, in which these three factors cooperated to initiate the outburst during mining. Among the 84 outburst accidents in China during 2008–2018, the outbursts occurring in the crustal stress area, fault area and coal thickness variation area constituted 30.95%, 22.62% and 22.62%, respectively [7]. Therefore, investigating the mechanism for outbursts in the special

geological structural environment is of great significance for preventing and controlling the outbursts.

The special geological structural environment mainly includes the crustal stress zone, fault zone and coal thickness variation zone [8–11]. Previous researchers investigated the mechanism for outbursts in the crustal stress zone by the numerical simulation method and experimental tests, mainly from the perspective of energy instability [12–16]. In the crustal stress zone, the existence of deformed (tectonic) coal has an important effect on outbursts. The low strength of tectonic coals made the threshold value of critical gas pressure for outbursts lower than that of normal coals [17]. Lots of gas desorption volumes for deformed coals could provide enough energy for the migration of coal and gas during the outbursts' development [18]. The mechanical failure mechanism for a combination of deformed coal and normal coal was analyzed based on the force analysis, Mohr–Coulomb criterion and uncoordinated deformation equation, with the simulation result proving that the failure is more probable to generate at the interface between the deformed coal and normal coal [19]. By establishing the multi-physical coupling model, the distribution of horizontal stress, gas pressure and plastic failure for normal coal, deformed coal and a combination of deformed coal with normal coal was simulated [20]. The results of numerical simulation showed that the combination of deformed coal and normal coal has a larger horizontal tensile stress and plastic failure zone, whose outburst energy is 149 times than that of normal coal.

Meanwhile, massive, interesting investigations focused on the mechanism for fault-induced outbursts [21–25]. From the perspective of geological factors, the existence of tectonic coal, lower permeability and higher gas content in the footwalls of a reverse fault were the principal factors causing the outbursts [23,25,26]. From the perspective of mining disturbance, the dynamic evolution of stress, gas pressure, permeability and plastic failure mainly controlled the outbursts [27–30]. Wang et al. [22,31] combined physical simulation and numerical simulation to study the stress evolution around the fault and illustrate the mechanism for fault slips induced by coal mining. The results indicated that the higher horizonal stress is the main reason for fault slips, which provides the dynamic pressure source for the outburst occurrence. Cai et al. [21] illustrated the mechanism for fault-induced coal bursts under mining-induced static and dynamic stresses using experimental tests, numerical modelling and in-suit micro-seismic monitoring. Compared with investigations into the mechanism for outbursts in the ground stress area and fault area, the investigation of the outburst mechanism in the coal thickness variation area is insufficient. Ma et al. [32] studied the effect of coal thickness on the strength, elastic modulus and energy evolution of a coal–rock combination. Álvarez-Fernández et al. [33] employed numerical modelling to analyze the effect of local change in coal seam thickness on the surrounding stress. However, how the stress, gas pressure and plastic failure zone evolve, and what the mechanism for energy instability in outbursts is in the coal seam thickening area during mining were rarely reported and still need further investigation.

To illustrate the mechanism for outbursts occurring in the coal thickening areas, a coupled multi-field model was first established by considering the stress–strain field, gas transport field and damage field (in Section 2). Based on the multi-field model, the evolution of stress, gas pressure and plastic failure zone under different variation gradients and amplitudes of coal thickness were investigated by using numerical simulation results (in Section 3). The mechanism for outbursts occurring in the coal thickness variation areas was then discussed, combined with the numerical simulation results and the energy principle of outbursts (in Section 4). Finally, the conclusions in Section 5 were drawn, including that the research could provide the theoretical support required to prevent and control outbursts in coal seam thickening area during mining.

2. Theory

Mining disturbance is the direct cause of outbursts, which change the distribution of stress and gas pressure in front of the mining roadway [34]. The distribution of stress and gas pressure is related to the gas flow in the coal seams. Therefore, the multi-field coupling model is the key to understanding the mechanism for outbursts in coal seam thickening areas. In this study, a multi-field coupling model was established by considering the stress–strain field, gas transport field, failure criterion and the following assumptions.

1. Coal is an homogeneous and isotropic material, with a dual porosity including matrix pore and fracture;
2. Methane is taken as the only and ideal gas in the coal seam, whose flow in the coal fracture and matrix obeys Darcy's law and Fick diffusion law, respectively;
3. The effect of time on gas adsorption and desorption is neglected, which means that the gas adsorption and desorption occurs instantaneously;
4. The effect of water on permeability is negligible.

2.1. Governing Equation of Coal Deformation

The stress-balance equation and geometric equation of coal deformation can be expressed as [35,36]:

$$\begin{cases} \sigma_{ij,i} + F_j = 0 \\ \varepsilon_{ij} = \frac{1}{2}(u_{i,j} + u_{j,i}) \end{cases} \tag{1}$$

where subscripts i, j stand for the main direction; F_j means the body stress in the j direction; ε_{ij} means the strain component; u_i is the displacement component in the i direction; and u_j is the displacement component in the j direction.

With the mining process, the effective stress varied with the change of gas pressure. The strain of coal occurred due to the variation of effective stress, gas adsorption and desorption. Considering the above factors comprehensively and Hooke's law, the constitutive equation between the stress and strain can be written as [37,38]:

$$\varepsilon_{ij} = \frac{1}{2G}\sigma_{ij} - \left(\frac{1}{6G} - \frac{1}{9K}\right)\sigma_{kk}\delta_{ij} + \frac{\alpha_m p_m \delta_{ij} + \alpha_f p_f \delta_{ij}}{3K} + \frac{\varepsilon_s \delta_{ij}}{3} \tag{2}$$

where σ_{ij} is the total stress tensor; G and K indicate the shear modulus and bulk modulus of coal; σ_{kk} is the sum of the three normal stress component; δ_{ij} is the Kronecker delta ($\delta_{ij} = 1$ as $i = j$ and 0 in other cases); α_f and α_m are the effective coefficient for the fracture and matrix; p_f and p_m are the gas pressure in the fracture and matrix; and ε_s is the sorption-induced volumetric strain of the coal body.

The parameters in Equation (2) can be expressed as [39,40]:

$$G = \frac{E}{2(1+v)} \tag{3}$$

$$K = \frac{E}{3(1-2v)} \tag{4}$$

$$\alpha_m = \frac{K}{K_m} - \frac{K}{K_s} \tag{5}$$

$$\alpha_f = 1 - \frac{K}{K_m} \tag{6}$$

$$K_m = \frac{E_m}{3(1-2v)} \tag{7}$$

$$K_s = \frac{K_m}{1 - 3\varnothing_m(1-v)/2(1-2v)} \tag{8}$$

$$\varepsilon_s = \frac{\varepsilon_{max} p_m}{p_m + p_L} \tag{9}$$

where E and v are the Young's modulus and Poisson's ratio of coal; E_m, K_m and K_s are the elastic modulus of coal matrix, bulk modulus of coal matrix and bulk modulus of coal skeleton [41]; $\varnothing_m$ is the porosity of coal matrix; ε_{max} is the maximum sorption-induced volumetric strain of the coal body; and p_L is the Langmuir-type pressure of the sorption-induced volumetric strain.

By substituting Equation (2) into Equation (1), the Navier-type equation was modified as [42]:

$$Gu_{i,jj} + \frac{G}{1-2v} u_{j,ji} - \alpha_m p_{m,i} - \alpha_f p_{f,i} - K\varepsilon_{s,i} + F_i = 0 \tag{10}$$

The Equation (10) is a couple model of coal deformation, which comprehensively considers the effects of gas pressure variation in coal fracture and matrix and sorption-induced volumetric strain.

2.2. Governing Equation of Gas Flow

The governing equation of gas flow in the coal includes the gas diffusion equation and gas seepage equation. The gas diffusion occurs in the coal matrix, while the seepage occurs in the coal fracture. Based on the Fick diffusion law, the continuous equation of gas flow in the coal matrix can be expressed as [40]:

$$\frac{\partial m_m}{\partial t} + \frac{M}{\tau RT}\left(p_m - p_f\right) = 0 \tag{11}$$

where M is the gas molar mass; τ is the coefficient of gas transfer between coal fracture and matrix; R is the ideal gas constant; T is the gas temperature; and m_m is gas mass per unit volume in the coal matrix, which can be expressed as:

$$m_m = \frac{abp_m}{1+bp_m}\frac{M}{V_{std}}\rho_c + \frac{M}{RT}p_m\varnothing_m \tag{12}$$

where a and b are the gas adsorption constant; V_{std} is the gas molar volume; and ρ_c is the density of coal. By substituting Equation (12) into Equation (11), the matrix gas pressure can be expressed as:

$$\frac{\partial p_m}{\partial t} = \frac{-\left(p_m - p_f\right)\left(V_{std} \times (1+bp_m)^2\right)}{\tau\left(abRT\rho_c + \varnothing_m V_{std} \times (1+bp_m)^2\right)} \tag{13}$$

Based on the Darcy's law, the gas mass conservation in the coal fracture can be expressed as [43]:

$$\frac{\partial m_f}{\partial t} - \nabla\left(\frac{M}{RT}p_f\frac{k}{\mu}\nabla p_f\right) = \frac{M\left(1-\varnothing_f\right)\left(p_m - p_f\right)}{\tau RT} \tag{14}$$

where μ is the dynamic viscosity of gas; k is the permeability in the coal fracture; $\varnothing_f$ is the fracture porosity; and m_f is the gas mass in the coal fracture, which can be expressed as:

$$m_f = \varnothing_f \frac{M}{RT}p_f \tag{15}$$

By substituting Equation (15) into Equation (14), the fracture gas pressure can be expressed as:

$$p_f \frac{\partial \varnothing_f}{\partial t} + \varnothing_f \frac{\partial p_f}{\partial t} + \nabla\left(-\frac{k}{\mu} p_f \nabla p_f\right) = \frac{\left(1-\varnothing_f\right)\left(p_m - p_f\right)}{\tau} \tag{16}$$

The permeability in the coal fracture and fracture porosity are related with the effective stress and gas adsorption strain, which are evolved with the coal strain stage. During the mining process, the coal body in front of the roadway was damaged. Therefore, the equation of permeability in the residual strain stage was used, which can be expressed as [20]:

$$k = k_0(1+D\xi)exp\left\{-3C_f\left[\Delta\bar{\sigma} - \alpha_f \Delta p_f - \alpha_m \Delta p_m + \frac{K\Delta\varepsilon_s}{(1-f_m)}\right]\right\} \tag{17}$$

where D is the damage variable; ξ is the increase coefficient of permeability after the stress peak point; C_f is the fracture compressibility; and f_m is the proportion of matrix sorption deformation.

According to the cubic law between the fracture porosity and permeability, the equation of the fracture porosity can be expressed as:

$$\varnothing_f = \varnothing_{f0}(1+D\xi)^{1/3} exp\left\{-C_f\left[\Delta\bar{\sigma} - \alpha_f \Delta p_f - \alpha_m \Delta p_m + \frac{K\Delta\varepsilon_s}{(1-f_m)}\right]\right\} \tag{18}$$

where $\varnothing_{f0}$ is the initial fracture porosity.

2.3. Governing Equation of Coal Damage

The stress state and gas pressure state in front of the roadway varied with the coal mining activities. When the stress meets the maximum tensile failure criterion or Mohr–Coulomb criterion, the tensile failure or shear failure occurs in the coal body. The damage criterion function can be expressed as [13]:

$$\begin{cases} F_1 = -\sigma_3 - f_{t0} \\ F_2 = \sigma_1 - \sigma_3 \frac{1+\sin\varphi}{1-\sin\varphi} - f_{c0} \end{cases} \tag{19}$$

where F_1 and F_2 are the functions of stress state, and their zero value indicates that the coal suffers tensile damage and shear damage, respectively; σ_1 and σ_3 are the maximum principal stress and minimum principal stress; f_{t0} and f_{c0} are the uniaxial tensile strength and uniaxial compressive strength; and φ is the friction angle of the coal.

When the F_1 or F_2 equals to zero, the coal body experiences tensile failure or shear failure. Based on the elastic damage theory, the elastic modulus of coal would decrease linearly with the damage variable:

$$E_t = E(1-D) \tag{20}$$

where E_t is the elastic modulus of damaged coal; and D is the damage variable, which can be expressed as:

$$D = \begin{cases} 1 - \left|\frac{\varepsilon_{t0}}{\varepsilon_1}\right|^n & F_1 = 0 \text{ and } dF_1 > 0 \\ 0 & F_1 < 0 \text{ and } F_2 < 0 \\ 1 - \left|\frac{\varepsilon_{c0}}{\varepsilon_3}\right|^n & F_2 = 0 \text{ and } dF_2 > 0 \end{cases} \tag{21}$$

where ε_{t0} and ε_{c0} are the maximum tensile principal strain and the maximum compressive principal strain; n is a constant, here n = 2; and $dF_1 > 0$ and $dF_2 > 0$ mean the continuous loading state after the damage is reached.

Equations (10), (13), (16)–(19) and (21) constitute the multi-field coupling mathematic model of outbursts, which has been verified by our previous research [40,44].

3. Numerical Simulation

3.1. Geometric Models and Parameters

Comsol software was used to solve the multi-field governing equations in our study. To embed the theory into the Comsol platform, we used the solid mechanics and PDE modules built into the platform. The solid module can solve the stress–strain constitutive equation. The PDE modules can solve the gas seepage and gas diffusion equations. The model diagram is shown in Figure 1, which is composed with the coal seam at the middle part and rock layers at the upper and lower parts. The initial excavation height of the roadway is 3 m. The excavation width of the roadway is 4 m. The vertical stress with 10 MPa is loaded under the roof, while other sides are supported by the roller. The gas pressure at the face of the roadway is set as 0.1 MPa. The center line of the roadway is defined as the monitoring line. The location of coal thickness variation is 80 m away from the initial excavation location. Two modes of coal thickness variation were simulated to investigate the evolution characteristics of stress, gas pressure and plastic failure zone. One mode is different change gradients of coal thickness with the same variation amplitude from 3 m to 7 m. The change gradient can be determined by the length of the thickening transition zone (Figure 1A). For the same change amplitude, the gradient increases with the decrease in the length of the thickening transition zone. Another mode is different change amplitudes of coal thickness with the same change gradient, varying from 3 m to 5 m, 7 m, 9 m, 11 m and 13 m (Figure 1B). All constant parameters used in the model are summarized in Table 1.

Table 1. Constant parameters used in the simulation model.

Name	Symbol	Value
Young's module of coal	E	2713 MPa
Young's module of rock	E_{s}	8423 MPa
Bulk module of coal matrix	K_m	12.4 MPa
Poisson's ratio of coal	v	0.32
Poisson's ratio of rock	v_r	0.25
Maximum sorption-induced strain	ε_{max}	0.011
Langmuir-type pressure of the sorption strain	p_L	5.14 MPa
Gas molar mass	M	16 g/mol
Ideal gas constant	R	8.31 J/(mol K)
Gas temperature	T	327.5 K
Coefficient of gas transfer	τ	794,880 s
Maximum gas adsorption capacity	a	5.278×10^{-2} m^3/kg
Adsorption constant	b	1.36×10^{-6} Pa^{-1}
Gas molar volume	V_{std}	0.0224 m^3/mol
Coal density	ρ_{c}	1400 kg/m^3
Rock density	ρ_{r}	2500 kg/m^3
Viscosity coefficient of methane	μ	1.84×10^{-5} Pa s
Matrix porosity	$\varnothing_m$	0.045
Initial fracture porosity	$\varnothing_{f0}$	0.012
Initial permeability	k_0	1×10^{-16} m^2
Fracture compressibility	C_f	1.36×10^{-6} Pa^{-1}
Increase coefficient of permeability	ξ	55
Proportion of matrix sorption deformation	f_m	0.1
Uniaxial tensile strength of coal	f_{t0}	0.5 MPa
Uniaxial compressive strength of coal	f_{c0}	3.47 MPa
Uniaxial tensile strength of rock	f_{st0}	3.53 MPa
Uniaxial compressive strength of rock	f_{sc0}	26.7 MPa
Internal friction angle of coal	φ	35°
Internal friction angle of rock	φ_r	40°

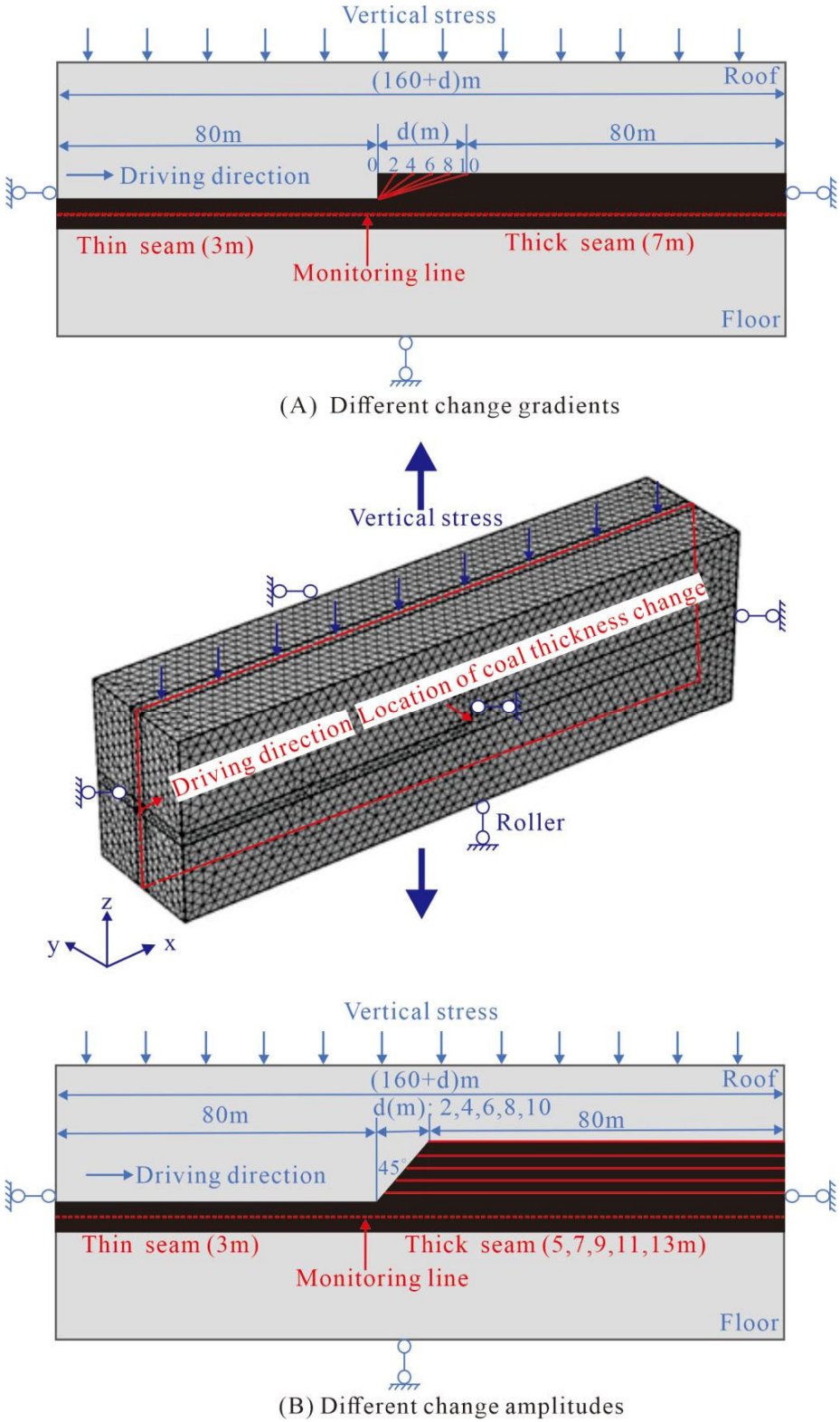

Figure 1. Diagram of coal thickness variation.

3.2. Analysis of Simulation Results

3.2.1. Characteristics of the Vertical Stress Evolution

To compare the different characteristics of the vertical stress evolution under the constant coal seam and coal thickness variation zone, due to the excavation disturbance, the simulation was conducted at different driving locations. Figures 2 and 3 present the

characteristics of the vertical stress evolution for the coal thickness variation, with different gradients and different amplitudes under different driving locations, respectively. The result that there is a stress peak in front of the driving face is similar to that found in the previous research [11]. There is also a stress concentration in the coal thickness variation transition zone when the driving location is 30 m and 50 m, far away from 80 m. This stress concentration is the original stress in the thickness variation transition zone and is related to the effective elastic module in the coal thickness variation zone [45].

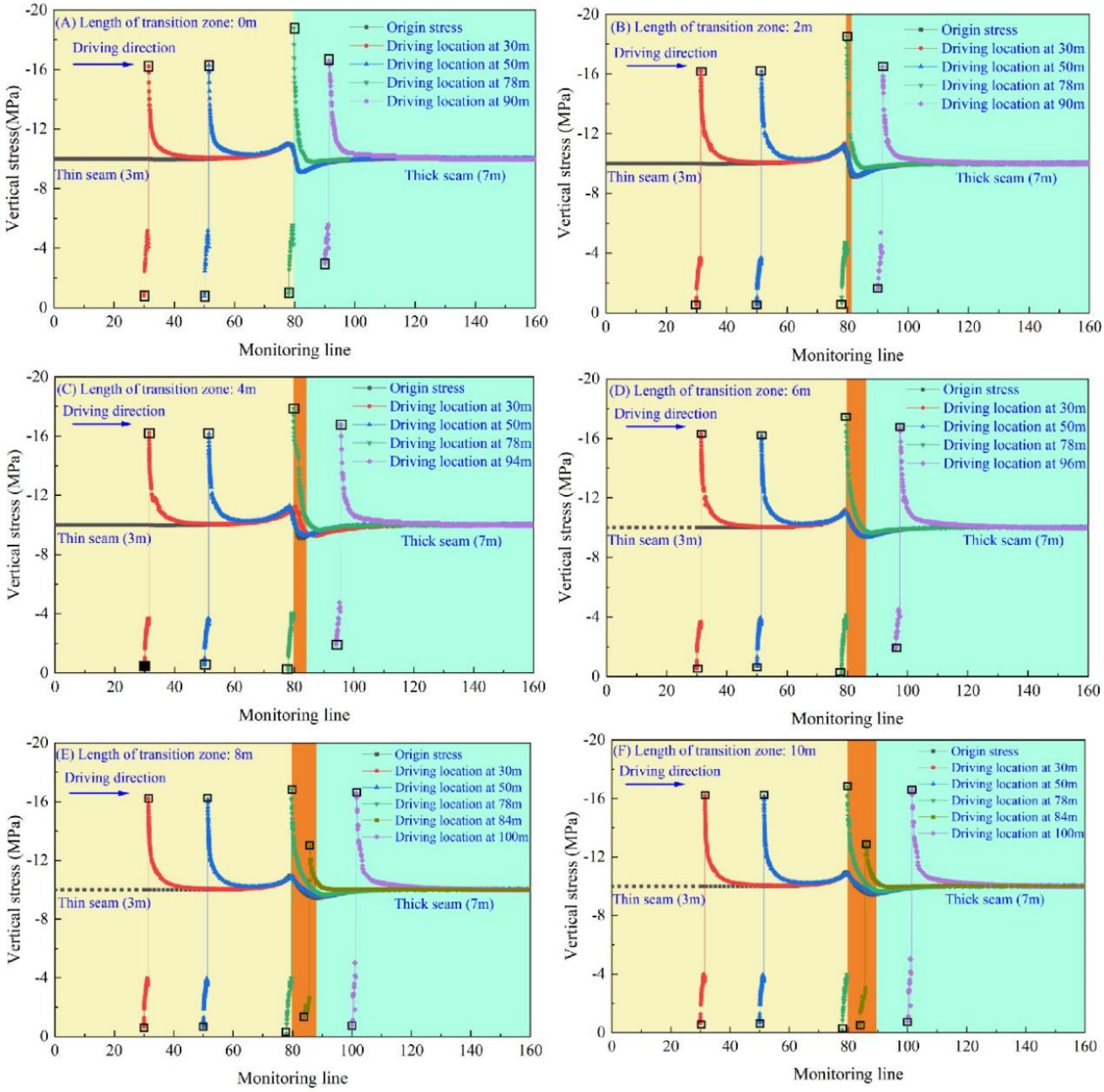

Figure 2. The evolution of stress under different coal thickness variation gradients.

Compared with the stress peak in the constant coal thickness, whether thick coal seam or thin coal seam, the stress peak in the coal thickness variation transition zone is higher when the driving location is at 78 m. However, the stress peak is lower when the driving location is in the coal thickness variation zone shown in Figure 2E,F and Figure 3. The result may be related to the uneven distribution of the elastic module of coal in the coal thickness variation zone [45]. The stress peak at the coal thickness variation transition

zone is also different for different variation gradients and variation amplitudes when the driving location is at 78 m. Figure 4 further compares the influence of coal thickness change gradients and change amplitudes on the stress peak when the driving location is at 78 m. From Figure 4A, the maximum vertical stress ranges from 18.8 MPa to 16.9 MPa, decreasing with the decrease in the coal thickness variation gradient; while the maximum vertical stress ranges from 16.2 MPa to 19.3 MPa, increasing with the increase in the coal thickness variation amplitude (Figure 4B). This phenomenon indicates that outbursts occur more easily in the coal thickness variation zone at higher gradients or higher amplitudes.

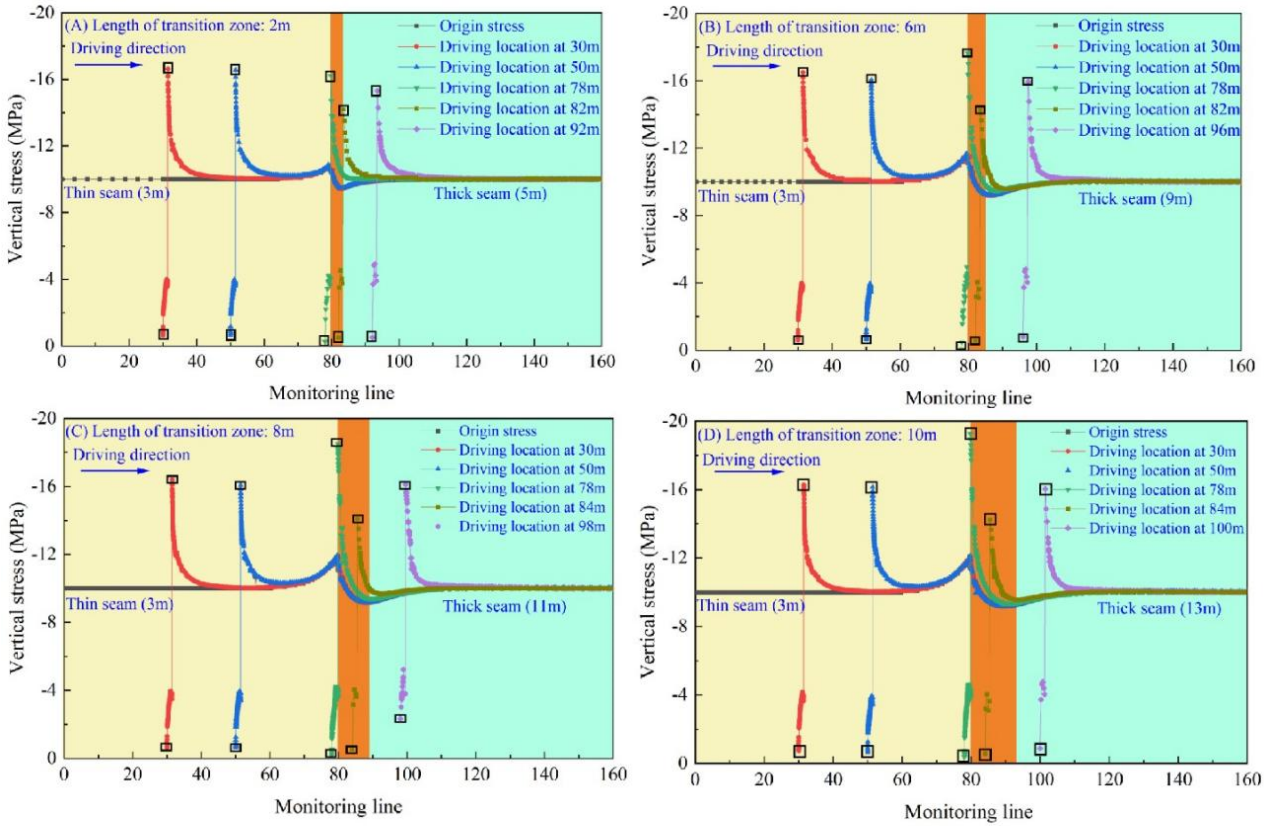

Figure 3. The evolution of stress under different coal thickness variation amplitude.

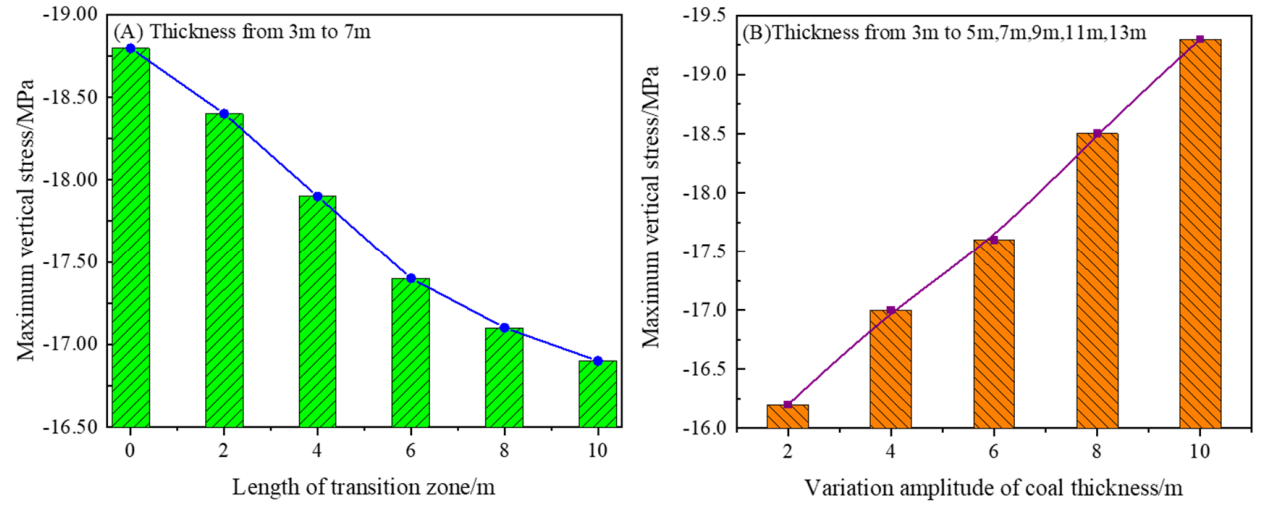

Figure 4. Influence of coal thickness variation gradient and amplitude on the peak stress at 78 m driving location.

3.2.2. Distribution of the Plastic Failure Zone

The coal thickness variation not only influences the stress evolution, but also damages the coal adjacent to the coal thickness variation transition zone, which can be revealed by the plastic failure. Figures 5 and 6 show the distribution of plastic failure under different variation gradients and variation amplitudes when the driving face is at 78 m from the coal thickness variation transition zone. The plastic failure is biggest close to the driving face and decreases gradually with distance.

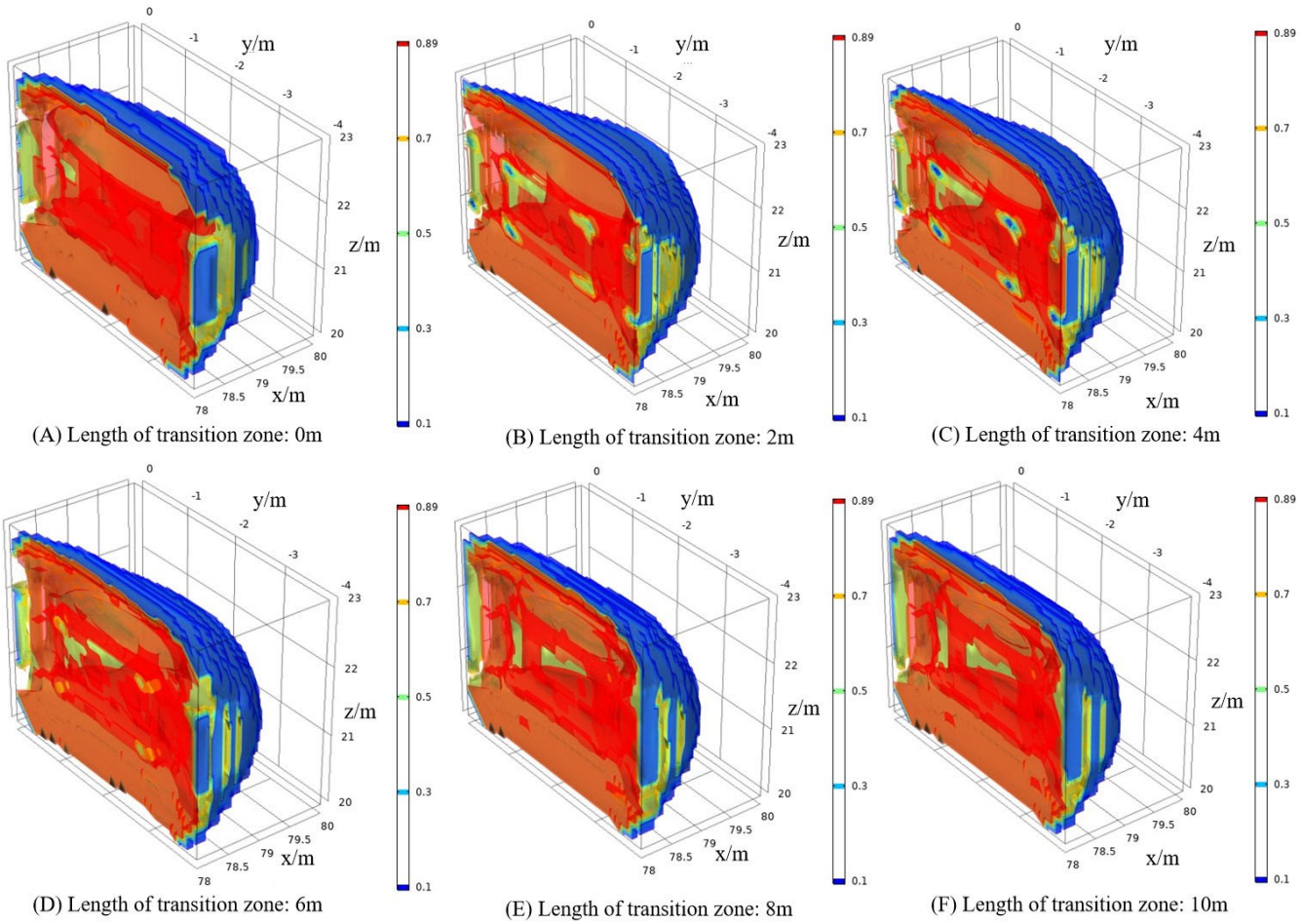

Figure 5. Plastic failure zone affected by different coal thickness variation gradients at 78 m driving location.

In order to compare the influence of coal thickness variation gradients and variation amplitudes on the plastic failure zone, the plastic deformation volume of coal was obtained by calculating the volume fraction of the damage variable greater than zero, as depicted in Figure 7. The plastic deformation volume of coal decreases from 12.48 m^3 to 10.82 m^3 with a decrease in the coal thickness variation gradient (Figure 7A) and increases from 11.13 m^3 to 12.68 m^3 with an increase in the coal thickness variation amplitude (Figure 7B). This result demonstrates that the damage to the coal in front of the driving face is more serious at the coal thickness variation zone at higher gradients or higher amplitudes.

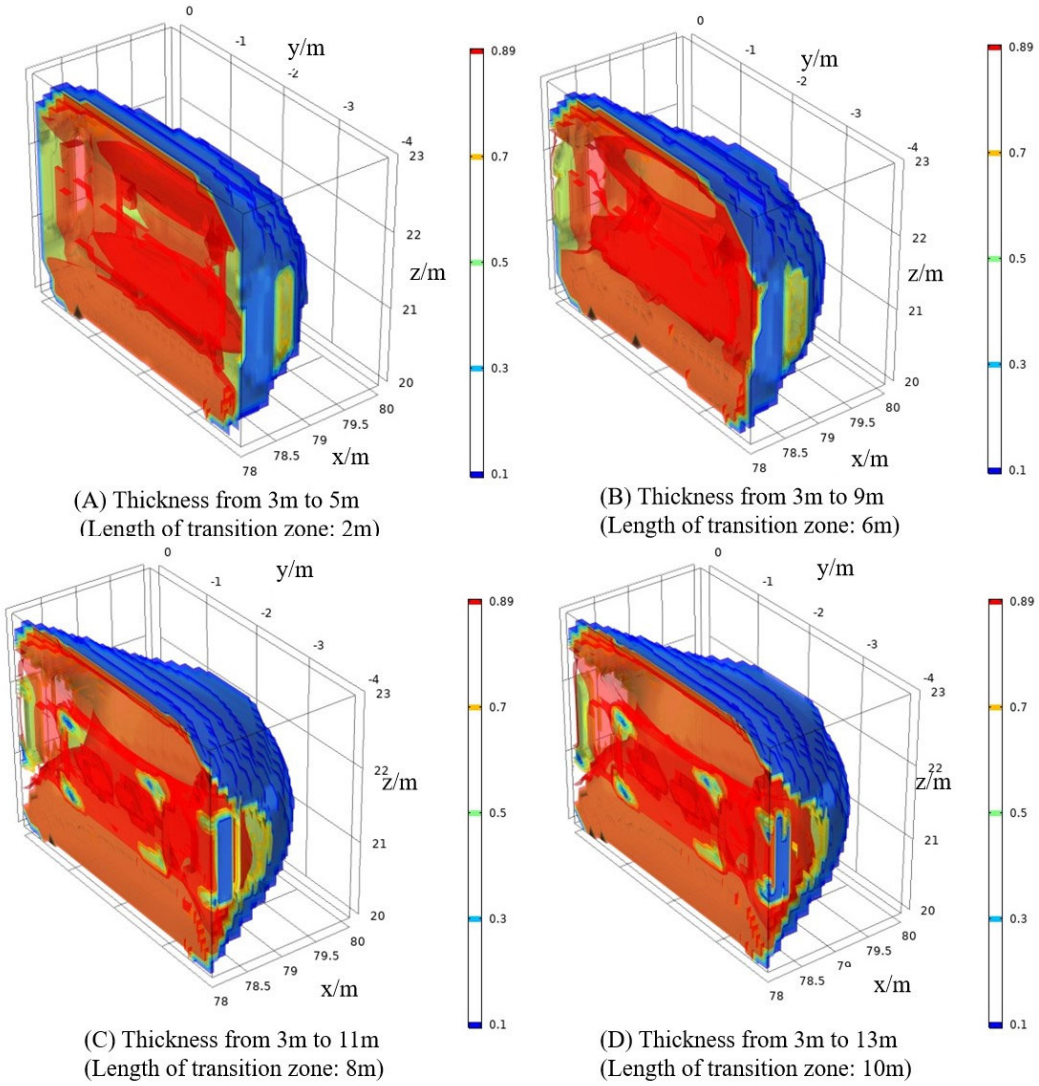

Figure 6. Plastic failure zone affected by different coal thickness variation amplitudes at 78 m driving location.

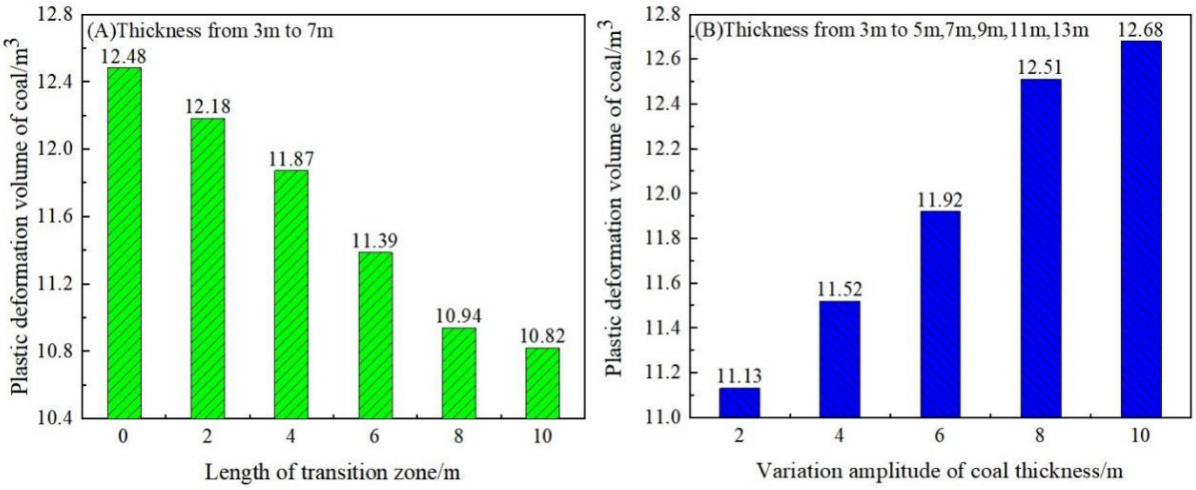

Figure 7. Influence of coal thickness variation gradient and amplitude on the plastic deformation volume of coal at 78 m driving location.

3.2.3. Characteristics of the Gas Pressure Evolution

The influence of excavation on gas pressure is related to the distance to the heading face. The gas pressure increases gradually from 0.1 MPa at the driving face to the initial gas pressure, forming the gas pressure gradient between the driving face and coal seam [13]. The gas pressure gradient is related to the gas seepage and gas expansion energy that contribute to an outburst. According to the rules of outburst prevention and control, the minimum distance for anti-burst measures should be 5 m ahead of the driving face. Therefore, the 83 m point in the monitoring line is regarded as the monitoring point.

The evolution of gas pressure in the matrix and in the fracture at the monitoring point is shown in Figure 8. The gas pressure in the fracture declines quickly in the initial stage and then declines gradually (Figure 8B,D), which may be due to lots of the free gas in the fracture and some desorption gas being released at the initial stage, followed by a slow gas flow for the decreasing free gas and the gas pressure gradient between the fracture and the matrix, while the gas pressure in the matrix declines steadily (Figure 8A,C). With the increase in time, the impact of coal thickness variation on gas pressure can be clearly seen. From Figure 8A,B, the gas pressure in the matrix and fracture at 30 min decreases with the decrease in the coal thickness variation gradient, which indicates that the higher coal thickness variation gradient causes more gas to be retained in the coal seam. From (Figure 8C,D), the gas pressure in the matrix and fracture at 30 min increases with the increase in the coal thickness variation amplitude, which indicates that the higher coal thickness variation amplitude also causes more gas to be retained in the coal seam. The results are related to the influence of coal thickness variation on stress distribution. The higher the coal thickness variation gradient or amplitude, the higher the peak stress in the coal thickness variation zone [46]. Higher stress leads to lower permeability, causing more gas to be retained and higher gas pressure in the zone [47,48].

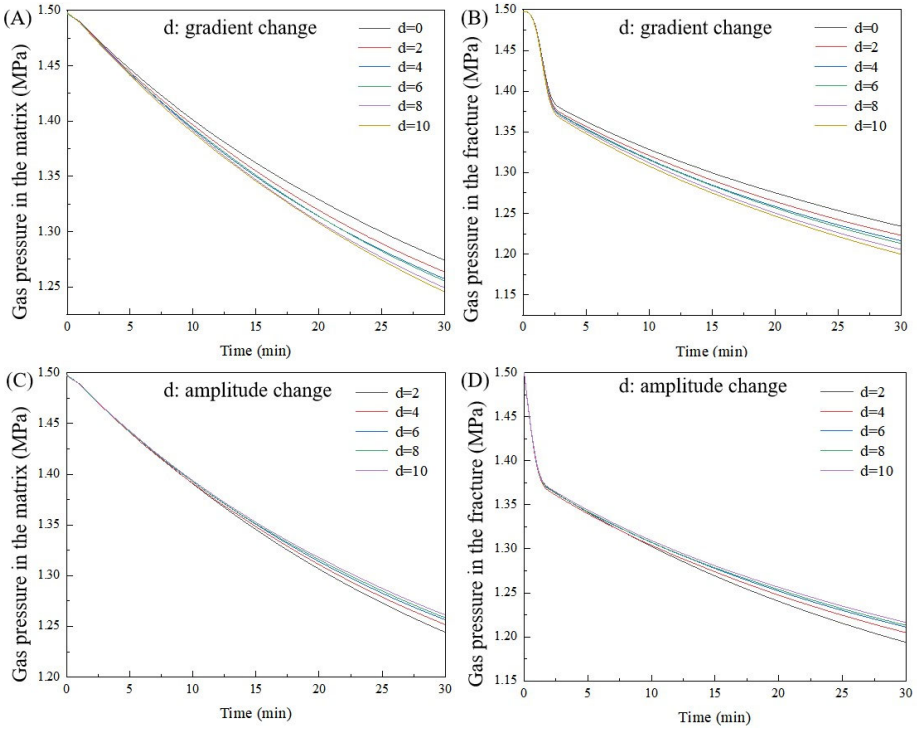

Figure 8. Influence of coal thickness variation gradient and amplitude on gas pressure at 78 m driving location (**A**): Evolution of gas pressure in the matrix in different coal thickness variation gradients; (**B**): Evolution of gas pressure in the fracture in different coal thickness variation gradients; (**C**): Evolution of gas pressure in the matrix in different coal thickness variation amplitudes; (**D**): Evolution of gas pressure in the fracture in different coal thickness variation amplitudes).

4. Discussion

From the simulation results, the coal thickness variation has an important effect on the distribution of stress, gas pressure and the plastic failure zone ahead of the driving face, which relate to the occurrence of outbursts. In recent years, the degree of outburst initiation has been evaluated from the perspective of energy principles [1]. The energy contributing to the outburst initiation mainly includes the elastic energy and free gas expansion energy, called outburst energy. The elastic energy relates to the ground stress in three directions, the elastic module and Poisson's ratio of coal, which can be expressed as:

$$E_e = \frac{{\sigma_1}^2 + {\sigma_2}^2 + {\sigma_3}^2 - 2\nu(\sigma_1\sigma_2 + \sigma_1\sigma_3 + \sigma_2\sigma_3)}{2E} \tag{22}$$

where E_e is the elastic energy per unit volume of coal; and σ_1, σ_2, σ_3 are the principal stresses in three directions.

The free gas expansion energy relates to the fracture gas pressure, which can be expressed as:

$$E_g = \frac{p_a V_g}{\gamma_n - 1}\left[\left(\frac{p_f}{p_a}\right)^{\frac{\gamma_n - 1}{\gamma_n}} - 1\right] \tag{23}$$

$$V_g = \frac{V_p p_f T_0}{T p_a Z} \tag{24}$$

where E_g is the free gas expansion energy per unit mass; V_g is the free gas content calculated by Equation (24); p_a is the atmospheric pressure; γ_n is the adiabatic coefficient, 1.25 [6]; V_p means the pore volume per unit mass; T_0 and T are the temperature under the standard condition and coal seam; and Z means the gas compressibility coefficient.

According to the rule that the distance of overhead cover required for local anti-burst measures at the mining face is 10 m, the outburst energy is analyzed for areas 10 m ahead of the heading face. The simulation results for stress and fracture gas pressure are used to calculate the elastic energy and free gas expansion energy. The coal thickness varying from 3 m to 13 m with a 10 m transition area is used as an example to illustrate the evolution of outburst energy under different driving locations. Figure 9 presents the variation of elastic energy and free gas energy in areas 10 m ahead of the heading face. From Figure 9, the elastic energy and the free gas expansion energy increase from 1.85 MJ and 24.19 MJ when the driving location is 30 m to 1.94 MJ and 50.57 MJ when the driving location is 78 m close to the coal thickness variation transition zone. This result indicates the coal thickness variation has an important impact on the free gas expansion energy.

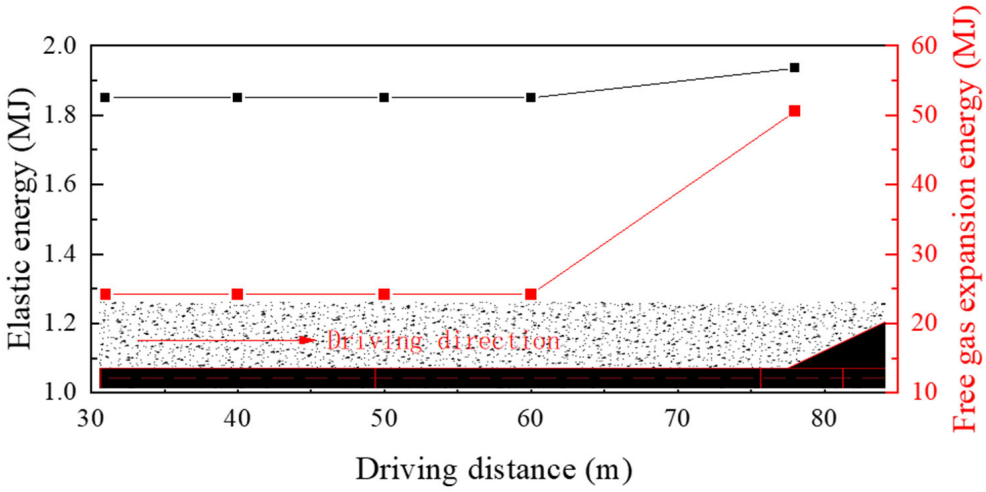

Figure 9. Evolution law of coal outburst potential within 10 m in front of roadway.

In order to further illustrate the influence of the coal thickness variation gradient and amplitude on the outburst energy, the free gas expansion energy per unit mass was calculated in areas 10 m ahead of the heading face at 78 m, as shown in Figure 10. With the decrease in the coal thickness variation gradient, the free gas expansion energy per unit mass of coal ranges from 0.109 MJ/t to 0.104 MJ/t; while the free gas expansion energy per unit mass of coal ranges from 0.104 MJ/t to 0.108 MJ/t with the increase in the coal thickness variation amplitude. The results further prove that the higher the coal thickness variation gradient or amplitude is, the higher the outburst risk is.

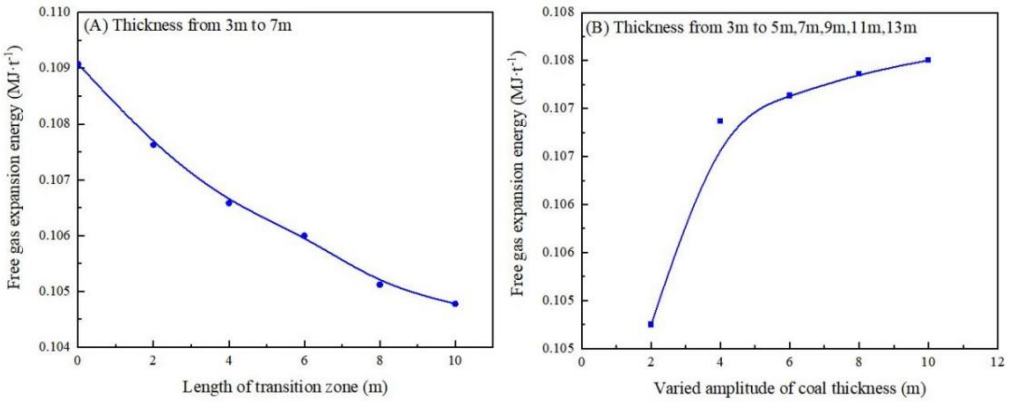

Figure 10. Influence of coal thickness variation gradient and amplitude on the free gas expansion energy of unit mass coal at 78 m driving location.

Based on the above discussion, the mechanism for outbursts in the coal seam thickening area can be inferred from Figure 11. Compared with the constant thickness coal seam, the stress peak is higher in the coal thickness variation transition zone, which increases the elastic energy. The higher stress peak also decreases the permeability, causing more free gas to be retained in the coal thickness variation zone, which increases the free gas expansion energy. In addition, the coal in the coal thickness variation zone may be deformed, which can contribute to the development of an outburst [20].

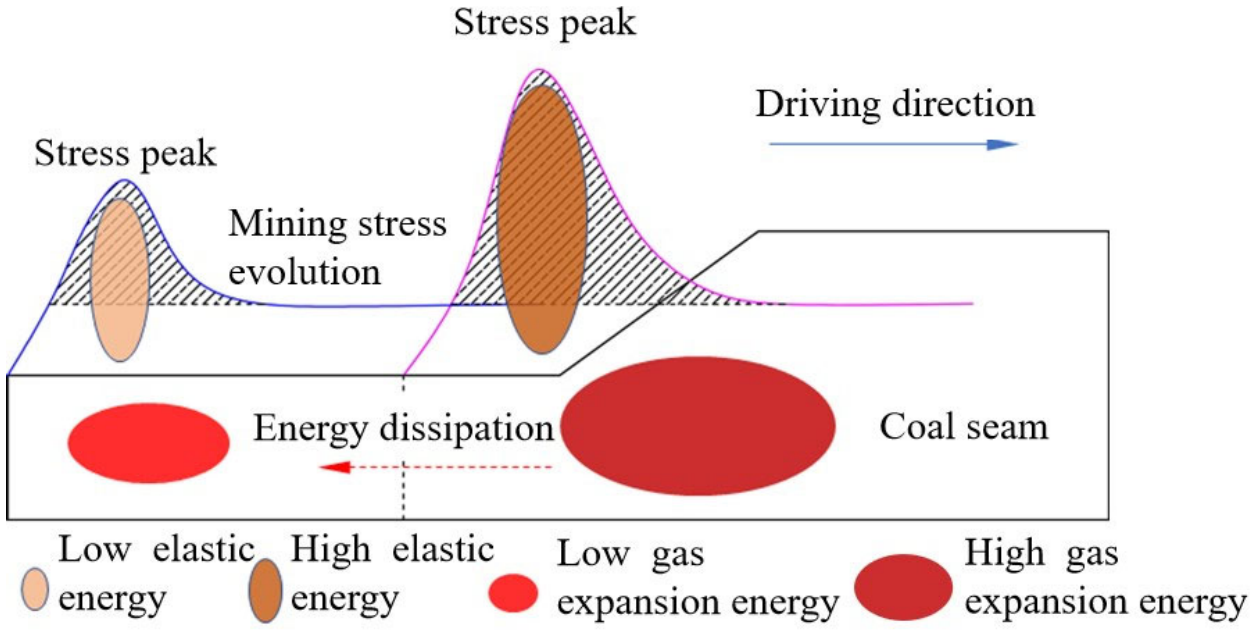

Figure 11. Schematic diagram of energy distribution and evolution during excavation of coal thickness variation region.

5. Conclusions

To illustrate the mechanism for outbursts in the coal thickening area during mining, a coupled multi-field model was first established by considering the stress–strain field, gas transport field and damage field. Based on the multi-field model, the evolution of stress, gas pressure and plastic failure zone under different variation gradients and amplitudes of coal thickness were investigated using numerical simulation. The mechanism for outbursts occurring in area of increasing coal thickness was discussed, combined with the numerical simulation results and the energy principle of outbursts. The main conclusions drawn are as follows.

(1) The stress peak at the transition zone of coal thickness variation during mining is higher than that at the constant coal thickness. The higher the coal thickness variation gradient or amplitude, the higher the stress peak at the transition zone of coal thickness variation.
(2) The plastic deformation volume of coal decreases with the decrease in the coal thickness variation gradient, and increases with the increase in the coal thickness variation amplitude.
(3) Affected by the higher coal thickness variation gradient or amplitude, the fracture gas pressure declines slower in the coal thickness variation zone, which increases the free gas expansion energy and the risk of outburst initiation.
(4) Compared with the constant thickness coal seam, outbursts occurring in the coal thickness variation zone are due to higher stress, higher gas pressure and lower coal strength, which forms higher elastic energy, higher free gas expansion energy and lower criteria for outburst initiation.

Based on the conclusions obtained from the results and discussion, the measures of advance pressure relief and gas extraction in the coal thickness variation zone should be further emphasized. In addition, other auxiliary measures should be taken to improve coal strength and restrain gas desorption to ensure mining safety in coal thickening areas.

Author Contributions: Methodology, Z.H.; Data curation, Y.F.; Writing—original draft, Z.L.; Writing—review & editing, L.S. All authors have read and agreed to the published version of the manuscript.

Funding: This research was funded by the Postdoctoral Research Foundation of China (Grant no. 2022M721450), the National Natural Science Fund of China (Grant nos. 52174187, 51704164, 52130409) and the Technology Innovation Fund of China Coal Research Institute (Grant no. 2020CX-I-07).

Data Availability Statement: Data is unavailable due to privacy or ethical restrictions.

Conflicts of Interest: The authors declare no conflict of interest.

References

1. Tu, Q.; Cheng, Y.; Xue, S.; Ren, T.; Cheng, X. Energy-limiting factor for coal and gas outburst occurrence in intact coal seam. *Int. J. Min. Sci. Technol.* **2021**, *31*, 729–742. [CrossRef]
2. Dutka, B. Effect of depth on the sorption capacity of coals affected by outburst hazard. *Fuel* **2021**, *306*, 121611. [CrossRef]
3. Black, D.J. Review of current method to determine outburst threshold limits in Australian underground coal mines. *Int. J. Min. Sci. Technol.* **2019**, *29*, 859–865. [CrossRef]
4. Yuan, L. Control of coal and gas outbursts in Huainan mines in China: A review. *J. Rock Mech. Geotech. Eng.* **2016**, *8*, 559–567. [CrossRef]
5. Xu, T.; Tang, C.A.; Yang, T.H.; Zhu, W.C.; Liu, J. Numerical investigation of coal and gas outbursts in underground collieries. *Int. J. Rock Mech. Min. Sci.* **2006**, *43*, 905–919. [CrossRef]
6. Shu, L.; Wang, K.; Liu, Z.; Zhao, W.; Zhu, N.; Lei, Y. A novel physical model of coal and gas outbursts mechanism: Insights into the process and initiation criterion of outbursts. *Fuel* **2022**, *323*, 124305. [CrossRef]
7. Xie, X.; Shen, S.; Fu, G.; Shu, X.; Hu, J.; Jia, Q.; Shi, Z. Accident case data–accident cause model hybrid-driven coal and gas outburst accident analysis: Evidence from 84 accidents in China during 2008–2018. *Process Saf. Environ. Prot.* **2022**, *164*, 67–90. [CrossRef]
8. Xu, C.; Yang, G.; Wang, K.; Fu, Q. Uneven stress and permeability variation of mining-disturbed coal seam for targeted CBM drainage: A case study in Baode coal mine, eastern Ordos Basin, China. *Fuel* **2021**, *289*, 119911. [CrossRef]

9. An, Y.; Zhang, N.; Zhao, Y.; Xie, Z. Field and numerical investigation on roof failure and fracture control of thick coal seam roadway. *Eng. Fail. Anal.* **2021**, *128*, 105594. [CrossRef]
10. Hou, C.; Zhang, Y.; Yan, Y. Effects of coal seam dip angle on the outburst in coal roadway excavation. *Int. J. Min. Sci. Technol.* **2019**, *29*, 757–764. [CrossRef]
11. Xue, D.; Wang, J.; Zhao, Y.; Zhou, H. Quantitative determination of mining-induced discontinuous stress drop in coal. *Int. J. Rock Mech. Min. Sci.* **2018**, *111*, 1–11. [CrossRef]
12. Zhou, B.; Xu, J.; Peng, S.; Yan, F.; Gao, Y.; Li, Q.; Cheng, L. Effects of geo-stress on the dynamic response of multi-physical field parameters during coal and gas outbursts under true triaxial stress. *Int. J. Rock Mech. Min. Sci.* **2021**, *142*, 104759. [CrossRef]
13. Zhao, Y.; Lin, B.; Liu, T.; Zheng, Y.; Kong, J.; Li, Q.; Song, H. Mechanism of multifield coupling-induced outburst in mining-disturbed coal seam. *Fuel* **2020**, *272*, 117716. [CrossRef]
14. Zhang, H.; Lu, C.; Liu, B.; Liu, Y.; Zhang, N.; Wang, H. Numerical investigation on crack development and energy evolution of stressed coal-rock combination. *Int. J. Rock Mech. Min. Sci.* **2020**, *133*, 104417. [CrossRef]
15. Kursunoglu, N.; Onder, M. Application of structural equation modeling to evaluate coal and gas outbursts. *Tunn. Undergr. Space Technol.* **2019**, *88*, 63–72. [CrossRef]
16. Liu, Q.; Wang, E.; Kong, X.; Li, Q.; Hu, S.; Li, D. Numerical simulation on the coupling law of stress and gas pressure in the uncovering tectonic coal by cross-cut. *Int. J. Rock Mech. Min. Sci.* **2018**, *103*, 33–42. [CrossRef]
17. Tu, Q.; Xue, S.; Cheng, Y.; Zhang, W.; Shi, G.; Zhang, G. Experimental study on the guiding effect of tectonic coal for coal and gas outburst. *Fuel* **2022**, *309*, 122087. [CrossRef]
18. Lei, Y.; Cheng, Y.; Ren, T.; Tu, Q.; Shu, L.; Li, Y. The energy principle of coal and gas outbursts: Experimentally evaluating the role of gas desorption. *Rock Mech. Rock Eng.* **2020**, *54*, 11–30. [CrossRef]
19. Lu, S.; Li, L.; Cheng, Y.; Sa, Z.; Zhang, Y.; Yang, N. Mechanical failure mechanisms and forms of normal and deformed coal combination containing gas: Model development and analysis. *Eng. Fail. Anal.* **2017**, *80*, 241–252. [CrossRef]
20. Lu, S.; Wang, C.; Liu, Q.; Zhang, Y.; Liu, J.; Sa, Z.; Wang, L. Numerical assessment of the energy instability of gas outburst of deformed and normal coal combinations during mining. *Process Saf. Environ. Prot.* **2019**, *132*, 351–366. [CrossRef]
21. Cai, W.; Dou, L.; Si, G.; Hu, Y. Fault-induced coal burst mechanism under mining-induced static and dynamic stresses. *Engineering* **2021**, *7*, 687–700. [CrossRef]
22. Wang, H.; Shi, R.; Deng, D.; Jiang, Y.; Wang, G.; Gong, W. Characteristic of stress evolution on fault surface and coal bursts mechanism during the extraction of longwall face in Yima mining area, China. *J. Struct. Geol.* **2020**, *136*, 104071. [CrossRef]
23. Li, W.; Ren, T.; Busch, A.; Den Hartog, S.A.M.; Cheng, Y.; Qiao, W.; Li, B. Architecture, stress state and permeability of a fault zone in Jiulishan coal mine, China: Implication for coal and gas outbursts. *Int. J. Coal Geol.* **2018**, *198*, 1–13. [CrossRef]
24. Li, H. Major and minor structural features of a bedding shear zone along a coal seam and related gas outburst, Pingdingshan coalfield, northern China. *Int. J. Coal Geol.* **2001**, *47*, 101–113. [CrossRef]
25. Cao, Y.; He, D.; David, C.G. Coal and gas outbursts in footwalls of reverse faults. *Int. J. Coal Geol.* **2001**, *48*, 47–63. [CrossRef]
26. Esen, O.; Özer, S.C.; Soylu, A.; Ramazani Rend, A.; Fişne, A. Geological controls on gas content distribution of coal seams in the Kınık coalfield, Soma Basin, Turkey. *Int. J. Coal Geol.* **2020**, *231*, 103602. [CrossRef]
27. Chen, Y.; Chu, T.; Chen, X.; Chen, P. Coupling of stress and gas pressure in dual porosity medium during coal seam mining. *Powder Technol.* **2020**, *367*, 390–398. [CrossRef]
28. Xia, T.; Zhou, F.; Liu, J.; Hu, S.; Liu, Y. A fully coupled coal deformation and compositional flow model for the control of the pre-mining coal seam gas extraction. *Int. J. Rock Mech. Min. Sci.* **2014**, *72*, 138–148. [CrossRef]
29. Guo, H.; Yuan, L.; Shen, B.; Qu, Q.; Xue, J. Mining-induced strata stress changes, fractures and gas flow dynamics in multi-seam longwall mining. *Int. J. Rock Mech. Min. Sci.* **2012**, *54*, 129–139. [CrossRef]
30. Yang, W.; Lin, B.; Qu, Y.; Li, Z.; Zhai, C.; Jia, L.; Zhao, W. Stress evolution with time and space during mining of a coal seam. *Int. J. Rock Mech. Min. Sci.* **2011**, *48*, 1145–1152. [CrossRef]
31. Wang, H.; Shi, R.; Song, J.; Tian, Z.; Deng, D.; Jiang, Y. Mechanical model for the calculation of stress distribution on fault surface during the underground coal seam mining. *Int. J. Rock Mech. Min. Sci.* **2021**, *144*, 104765. [CrossRef]
32. Ma, Q.; Tan, Y.; Liu, X.; Gu, Q.; Li, X. Effect of coal thicknesses on energy evolution characteristics of roof rock-coal-floor rock sandwich composite structure and its damage constitutive model. *Compos. Part B* **2020**, *198*, 108086. [CrossRef]
33. Álvarez-Fernández, M.I.; González-Nicieza, C.; Álvarez-Vigil, A.E.; Herrera García, G.; Torno, S. Numerical modelling and analysis of the influence of local variation in the thickness of a coal seam on surrounding stresses: Application to a practical case. *Int. J. Coal Geol.* **2009**, *79*, 157–166. [CrossRef]
34. Li, S.; Gao, M.; Yang, X.; Zhang, R.; Ren, L.; Zhang, Z.; Li, G.; Zhang, Z.; Xie, J. Numerical simulation of spatial distributions of mining-induced stress and fracture fields for three coal mining layouts. *J. Rock Mech. Geotech. Eng.* **2018**, *10*, 907–913. [CrossRef]
35. Cui, X.; Bustin, R.M. Volumetric strain associated with methane desorption and its impact on coalbed gas production from deep coal seams. *AAPG Bull.* **2005**, *89*, 1181–1202. [CrossRef]
36. Detournay, E.; Cheng, H.D. Fundamentals of poroelasticity. *Anal. Des. Methods* **1993**, *2*, 113–171.
37. Hosking, L.J.; Chen, M.; Thomas, H.R. Numerical analysis of dual porosity coupled thermo-hydro-mechanical behaviour during CO_2 sequestration in coal. *Int. J. Rock Mech. Min. Sci.* **2020**, *135*, 104473. [CrossRef]
38. Li, S.; Fan, C.; Han, J.; Luo, M.; Yang, Z.; Bi, H. A fully coupled thermal-hydraulic-mechanical model with two-phase flow for coalbed methane extraction. *J. Nat. Gas Sci. Eng.* **2016**, *33*, 324–336. [CrossRef]

39. Li, W.; Liu, J.; Zeng, J.; Leong, Y.-K.; Elsworth, D.; Tian, J. A fully coupled multidomain and multiphysics model considering stimulation patterns and thermal effects for evaluation of coalbed methane (CBM) extraction. *J. Pet. Sci. Eng.* **2022**, *214*, 110506. [CrossRef]
40. Fan, Y.; Shu, L.; Huo, Z.; Hao, J.; Li, Y. Numerical simulation of sectional hydraulic reaming for methane extraction from coal seams. *J. Nat. Gas Sci. Eng.* **2021**, *95*, 104180. [CrossRef]
41. Shu, L.; Yuan, L.; Li, Q.; Xue, W.; Zhu, N.; Liu, Z. Response characteristics of gas pressure under simultaneous static and dynamic load: Implication for coal and gas outburst mechanism. *Int. J. Min. Sci. Technol.* **2023**, *33*, 155–171. [CrossRef]
42. Ye, D.; Liu, G.; Gao, F.; Hu, Y.; Yue, F. A fractal model of thermal–hydrological–mechanical interaction on coal seam. *Int. J. Therm. Sci.* **2021**, *168*, 107048. [CrossRef]
43. Cui, G.; Liu, J.; Wei, M.; Shi, R.; Elsworth, D. Why shale permeability changes under variable effective stresses: New insights. *Fuel* **2018**, *213*, 55–71. [CrossRef]
44. Fan, Y.; Deng, C.; Zhang, X.; Li, F.; Wang, X.; Qiao, L. Numerical study of CO_2-enhanced coalbed methane recovery. *Int. J. Greenh. Gas Control* **2018**, *76*, 12–23. [CrossRef]
45. Zhu, N.; Zhang, L.; Shu, L.; Fan, X. Experimental study on microseismic precursory characteristics of coal and gas outburst and case analysis of early-warning. *Chin. J. Rock Mech. Eng.* **2018**, *37*, 1419–1429. [CrossRef]
46. Ma, Y.; Nie, B.; He, X.; Li, X.; Meng, J.; Song, D. Mechanism investigation on coal and gas outburst: An overview. *Int. J. Miner. Metall. Mater.* **2020**, *27*, 872–887. [CrossRef]
47. Li, Q.; Han, Y.; Liu, X.; Ansari, U.; Cheng, Y.; Yan, C. Hydrate as a by-product in CO_2 leakage during the long-term sub-seabed sequestration and its role in preventing further leakage. *Environ. Sci. Pollut. Res. Int.* **2022**, *29*, 77737–77754. [CrossRef]
48. Li, Q.; Wang, F.; Wang, Y.; Zhou, C.; Chen, J.; Forson, K.; Miao, R.; Su, Y.; Zhang, J. Effect of reservoir characteristics and chemicals on filtration property of water-based drilling fluid in unconventional reservoir and mechanism disclosure. *Environ. Sci. Pollut. Res. Int.* **2023**, *in press*. [CrossRef]